frontiers | Frontiers in Energy Research

TYPE Original Research
PUBLISHED 10 April 2024
DOI 10.3389/fenrg.2024.1369428

OPEN ACCESS

EDITED BY
Chengyuan Xu,
Southwest Petroleum University, China

REVIEWED BY
Yi Ding,
Southwest Petroleum University, China
Hu Guo,
China University of Petroleum, Beijing, China

*CORRESPONDENCE
Zou Yushi,
zouyushi@126.com

RECEIVED 12 January 2024
ACCEPTED 18 March 2024
PUBLISHED 10 April 2024

CITATION
Zening S, Zhanglong T, Junwen L, Qi A, Yushi Z, Shikang L and Ziwen Z (2024), Investigation into hydraulic fracture propagation behavior during temporary plugging and diverting fracturing in deep coal seam.
Front. Energy Res. 12:1369428.
doi: 10.3389/fenrg.2024.1369428

Investigation into hydraulic fracture propagation behavior during temporary plugging and diverting fracturing in deep coal seam

Sun Zening[1,2], Tan Zhanglong[1,2], Lin Junwen[1,2], An Qi[1,2], Zou Yushi[3]*, Liu Shikang[3] and Zhao Ziwen[3]

[1]China United Coalbed Methane Corporation Ltd, Beijing, China, [2]Provincial Center of Technology Innovation for Coalmeasure Gas Co-production, Taiyuan, China, [3]State Key Laboratory of Petroleum Resources and Prospecting, China University of Petroleum, Beijing, China

In this study, we conducted indoor temporary plugging and diverting fracturing (TPDF) experiments on samples of natural deep and shallow coal seams using a small-scale true triaxial fracturing simulation system. By integrating high-precision CT scanning technology and crack reconstruction techniques, and relying on the quantitative characterization of the crack complexity coefficient, we investigated the differences in internal structures between deep and shallow coal seam samples and the variations in the expansion of TPDF cracks. Furthermore, the study primarily focused on exploring the influence of temporary plugging agent (TPA) parameters (quantity and particle size) on the expansion patterns of TPDF cracks in deep coal seam coal-rock samples. The experimental results reveal that in shallow coal samples, artificially induced fractures are notably longer and extend to various surfaces of the samples. Conversely, in deep coal samples, the expansion of artificially induced fractures is influenced by well-developed cleavage and cleats. The crack complexity coefficient of artificial fractures in deep coal samples is 1.54 higher than that in shallow coal samples, with an increased crack width of 98 μm. However, the expansion distance of the fractures is shorter and does not extend to the S3 and S6 surfaces. Increasing the dosage of the TPA is advantageous for inducing frequent redirection of fractures and communication with previously untouched areas. When the dosage of the TPA is increased from 30 g/L to 60 g/L, the expansion distance of artificial fractures significantly increases, extending to various surfaces of the samples. The crack complexity coefficient increases by 1.1, and the crack width enlarges by 84 μm. Appropriate particle sizes of the TPA can effectively form seals. However, small particle sizes (200/400 mesh) struggle to seal initial fractures, while large particle sizes (10/20 mesh) can lead to excessive wellhead blockage, causing rapid shut-in pressure, destructive fracturing in deep coal samples, and the generation of a large amount of coal fines. This study holds significant guidance for the optimal selection of process parameters in the temporary plugging hydraulic fracturing of deep coal rock.

KEYWORDS

deep coal seam, fracture propagation, temporary plugging and diverting fracturing, temporary plugging agent, natural joint

1 Introduction

China, as a major coal-producing country, possesses abundant coalbed methane resources, contributing significantly to its vast coal resources and holding immense development potential. In the period from 2016 to 2018, the China National Petroleum Corporation (CNPC) evaluated the nation's coalbed methane resources, revealing that the coalbed methane resources at depths shallower than 2000m amount to approximately 29.82 × 10 × 12 m^3, with recoverable reserves estimated at around 12.51 × 10 × 12 m^3, ranking China third globally (Wuzhong et al., 2004; Huang et al., 2009; Sun et al., 2021; Huang et al., 2022; Qin et al., 2022). The Ordos Basin, where the Linxing-Shenfu Block is located, boasts a colossal share of coalbed methane resources, accounting for about one-third of the national total. Within the basin, coalbed methane resources at depths exceeding 1,000 m constitute 72%, highlighting the significance of deep coal seam exploitation (Li Huanhuan, 2020). Employing TPDF to enhance regional development has become an urgent necessity for increasing production in the block.

With the increasing depth of coalbed methane development, it has been observed that the fracturing crack propagation patterns in deep coal seams significantly differ from those in shallow ones. Deep coal reservoirs exhibit high fracturing pressures and strong heterogeneity, influenced by bedding planes, natural fractures, and cleat structures, resulting in complex crack propagation patterns (Kuuskraa and Wyman, 1993; Cheng and Guo, 2013; Gao et al., 2018; Xianqing et al., 2019; Zhang et al., 2019; Hou et al., 2021; Wu, 2022). Scholars both domestically and internationally have conducted research on the crack propagation patterns in deep coal and rock formations. Xue Haifei (Haifei et al., 2019) and others found that the characteristics of deep coalbed methane reservoirs differ significantly from shallow ones, with complex stress fields, variations in mechanical properties, and differences in coal structure all influencing to varying degrees the formation and development of fracturing cracks. Abass et al. (Abass, 1990) discovered that the greater the difference in horizontal stress, the more likely it is to form a single hydraulic fracture extending along the direction of maximum horizontal stress after fracturing. Yang Zhaozhong (Yang et al., 2017), through the establishment of a mathematical model for the stress distribution induced by vertical fractures in the horizontal plane, found that simultaneous fracturing can change the direction of the horizontal principal stress in deep coal seams, facilitating the reorientation and extension of hydraulic fractures to communicate with cleat fractures, forming a complex network of fractures. Wei Tao (Tao et al., 2018) studied the variation of the length and height of fracturing cracks with burial depth. Due to the exploitation of coalbed methane and the failure of initial fractures after the first fracturing, the single-well production shows a declining trend. To redirect the cracks and open up undeveloped areas in distant wells, temporary plugging and fracturing modification are required. Therefore, studying the propagation patterns and influencing factors of TPDF cracks and predicting the effects of temporary plugging and fracturing modification is of significant theoretical and practical importance.

Currently, there is relatively limited research on simulated indoor experiments of temporary plugging and fracturing in deep coal reservoirs. Moreover, studies on the plugging effect of temporary plugging agents within cracks mainly use a predetermined constant crack size and morphology method, unable to explore the dynamic changes in the actual internal crack expansion shapes and their impact on the plugging effect of the agents. In other words, temporary plugging and fracturing experiments are conducted independently of volume fracturing experiments, failing to fully utilize post-fracturing cracks. In this paper, a small-scale true triaxial fracturing simulation system was employed to conduct simulated experiments on TPDF on natural coal and rock samples measuring 80 × 80 × 100 mm^3. By integrating high-precision CT scanning technology with Solidworks-based three-dimensional crack reconstruction techniques, the differences in internal structures and crack propagation between deep and shallow coal seam strata were compared. Simultaneously, the effects of the dosage and particle size of temporary plugging agents on the propagation patterns of temporarily plugged diverted hydraulic fracturing cracks were investigated. The experimental results can provide guidance for optimizing the process parameters of TPDF in deep coal seam coal-rock formations.

2 Deep coal seam geological overview

The Linxing-Shenfu block has a large area and is characterized by a high level of structural implementation. The Taiyuan-Benxi Formation coal seam has an average thickness of 8m, with thickness ranging from 1.6 to 19.6 m. The average gas content of the coal seam is 13.3 m^3/t, ranging from 8 to 30.94 m^3/t. The primary structure of the coal body is the original-fracture structure, with mudstone as the main roof, including some sandstone. The overall average depth of the coal seam is greater than 1,700 m, with the southern part of Linxing having an overall depth greater than 2,000 m, while the northern part ranges from 1,700 to 2,000 m. Results from the Linxing-Shenfu reserve testing area align with geological expectations, boasting high gas content and substantial development potential (Fu et al., 2016; Guo, 2016; Lijun and Zhu, 2021; Yang, 2021).

Deep coal seams exhibit minor fractures and pores, experiencing high *in situ* stress, leading to high injection pressures during construction (Beugelsdijk et al., 2000; Guo, 2020; Zou et al., 2021; Jia et al., 2022). The maximum principal stress in the Linxing gas field averages 56 MPa, ranging from 38 to 62 MPa; the minimum principal stress averages 39 MPa, ranging from 21 to 45 MPa; the vertical stress averages 47MPa, ranging from 27 to 53 MPa. The deep coal seam has a low degree of pore development, low porosity, and an average pore size of 19.6 nm. Fracturing is crucial for improving pore-permeability conditions in deep coal seams to enhance production.

3 Simulation experiment of temporary plugging and turning hydraulic fracturing in deep coal seam rock

3.1 Test of mechanical properties of coal and rock in deep and shallow seams

The differences in the mechanical properties (Young's modulus, Poisson's ratio, etc.) between deep and shallow coal

FIGURE 1
Subsurface coal rock cuttings from wells LX2-48 and LX-42.

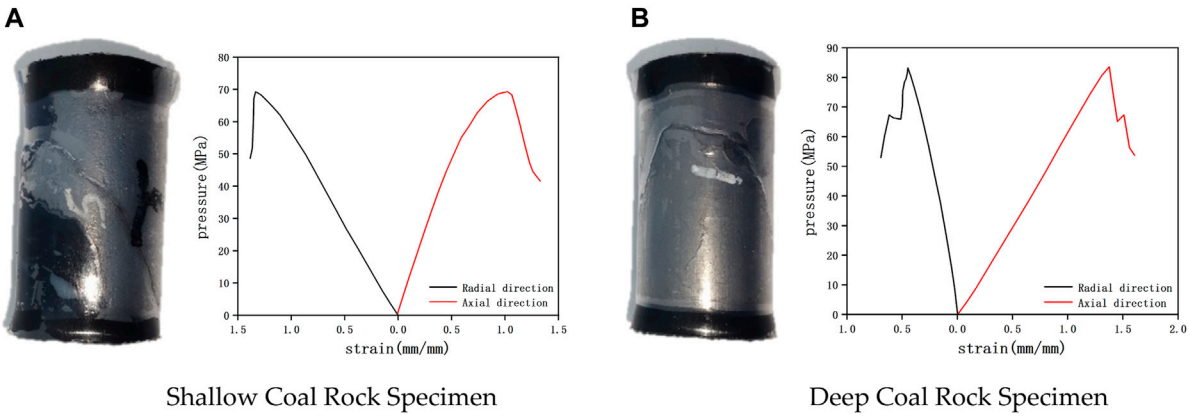

FIGURE 2
Specimen and corresponding stress-strain curve after triaxial compression test. **(A)** Shallow Coal Rock Specimen. **(B)** Deep Coal Rock Specimen.

seam rocks have significant implications for the formation and propagation of hydraulic fractures. In this study, two coal rock samples were selected from the Ordos Basin at burial depths of 850 m and 2,200 m, respectively. These samples were prepared into standard coal rock cores with dimensions of Φ25 mm × H50 mm for triaxial compression tests under full stress-strain conditions. Under reservoir temperature (60°C) and stress conditions (20 MPa), the mechanical parameters of reservoir rock, including Young's modulus, Poisson's ratio, and compressive strength, were determined through triaxial compression experiments. Two sets of triaxial compression tests were conducted, and the experimental specimens along with their corresponding stress-strain curves are depicted in Figure 2.

The mechanical test results, as shown in Table 1, reveal a comparison between the mechanical properties of coal and rock specimens from shallow and deep coal seams. It is evident that the elastic modulus of the coal and rock specimens from deep coal seams is 1.534 GPa higher than that of the shallow coal seams, with a corresponding decrease in Poisson's ratio by 0.082. This indicates that coal and rock specimens from deep coal seams are harder and less prone to deformation compared to those from shallow coal seams.

3.2 Experimental setup and sample preparation

Conducting indoor TPDF simulation experiments, we utilized a small-scale true triaxial fracturing simulation device, as illustrated in Figure 3 (Liu et al., 2000). The experimental samples for this study were extracted from the Linxing block of the Ordos Basin, with burial depths of 850 m and 2,200–2,300 m for comparison. The rock specimens were processed into 8080100 mm^3 rectangular prisms, featuring a centrally located blind hole with a diameter of 16 mm and a depth of 53 mm. A high-strength epoxy resin adhesive was employed to secure a steel pipe (wellbore) with an outer diameter of 15 mm, inner diameter of 8 mm, and length of 70 mm inside the blind hole, leaving a 5 mm open section at the bottom. Photographs of the coal rock samples before and after processing, along with a schematic diagram of the completed well, are depicted in Figure 4.

TABLE 1 Experimental results of triaxial compression.

Core	Length (mm)	Diameter (mm)	Weight (g)	Density (g/cm^3)	Confining pressure (MPa)	Deviatoric stress (MPa)	Modulus of elasticity (GPa)	Poisson's ratio
Shallow Coal Rock Specimen	50.73	25.48	35.09	1.36	20	82.657	5.898	0.296
Deep Coal Rock Specimen	49.92	25.65	32.66	1.27	20	69.204	4.364	0.378

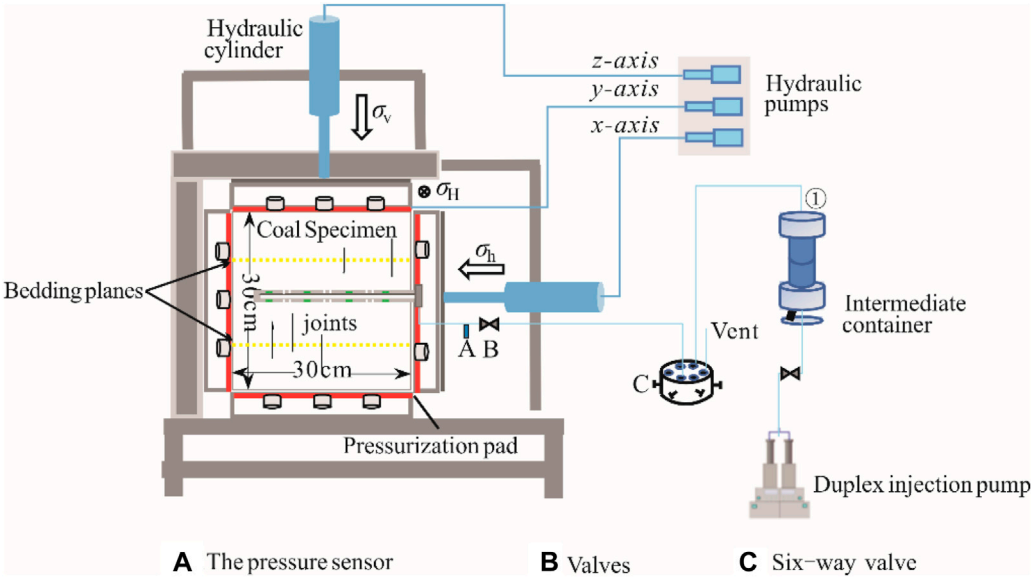

FIGURE 3
Small-scale true triaxial fracturing simulation system.

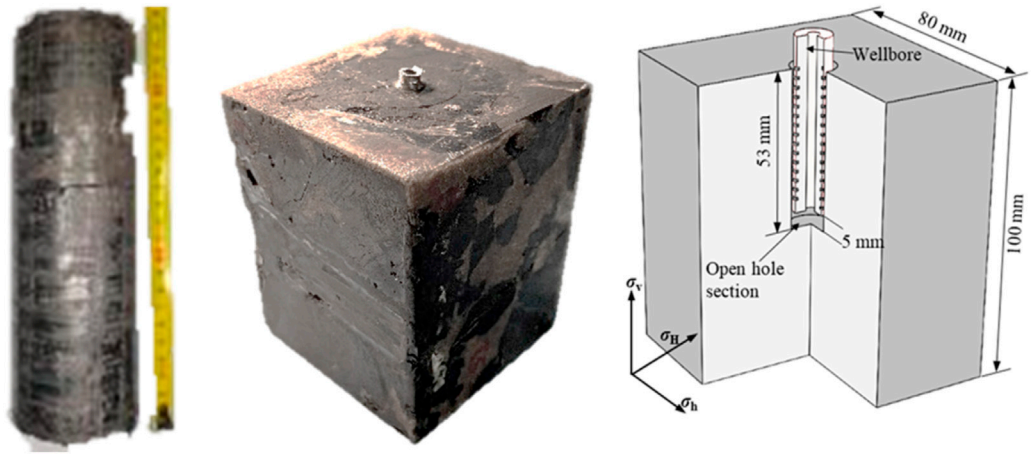

FIGURE 4
Coal and rock samples before and after processing, along with a schematic diagram of the completed well.

TABLE 2 Design of displacement parameters.

Construction parameters	Fracture Height/(m)	Injection rate/(mL/min)
Actual On-Site Parameters	13	15
Laboratory Parameters	0.05	0.00002

3.3 Experimental plan design

(1) Triaxial stresses

Due to the inability of the stress system in the indoor experimental equipment to replicate the actual stress conditions in reservoirs, this study employs the horizontal stress differential coefficient K_h (Xie et al., 2018) to calculate the relative magnitudes of the maximum and minimum horizontal principal stresses. These values are then utilized to design the triaxial stress parameters used in the indoor experiments. K_h is calculated using the following formula.

$$K_h = \frac{\sigma_H - \sigma_h}{\sigma_h} \tag{3.1}$$

In the Linxing-Shenfu Block, the maximum horizontal principal stress in coal seams at depths exceeding 2,000 m ranges from 38 to 62 MPa, while the minimum horizontal principal stress ranges from 21 to 45 MPa. Utilizing Eq. 3.1, the calculated K_h falls within the range of 0.378–0.810. Selecting K_h as 0.6, the experiment aims to simulate the stress conditions of deep coal seams. The designed maximum and minimum horizontal principal stresses are set at 16 MPa and 10MPa, respectively, with a vertical stress of 16 MPa.Applying the same method to the Linxing-Shenfu Block's coal seam at depths within 1,000 m yields a K_h range of 0.333–0.810. Opting for K_h as 0.6 to simulate the stress conditions of shallow coal seams, the designed maximum and minimum horizontal principal stresses are 8 and 5 MPa, respectively, with a vertical stress of 12 MPa.

(2)Displacement

Drawing upon the similarity criteria theory proposed by Liu et al. (Lu, 2017) for hydraulic fracturing simulation experiments, the injection parameters for indoor experiments are tailored to match the parameters used in on-site construction (refer to Table 2). The similarity criteria are defined by the following formula:

$$\begin{cases} \frac{c_L^3}{c_Q c_T} = 1, c_{K_L}\sqrt{\frac{c_L}{c_Q}} = 1, \frac{c\eta c_Q}{3} = 1 \\ \frac{c_L c_p}{\frac{c_{\sigma z}^0}{c_{ze}}} = \frac{c_p}{c_{Ee}} = \frac{c_{p_f}}{c_{Ee}} = 1, \\ \frac{c_L c_{Ee}^2}{2} = 1, \frac{c\gamma c_L}{c_{Ee}} = 1. \end{cases} \tag{3.2}$$

The similarity ratio coefficient, $c_V = V_{model}/V_{field}$ defined in the equation, where V_{model} represents the physical quantity of the experimental model, and V_{field} corresponds to the physical quantity of the corresponding on-site prototype. V represents single value conditional quantities such as L, E_e, Q, T, K_L, η, p, p_f, σ_{zz}^0, γ and K_{IC}.

(3) Fracturing Fluid viscosity

The selected viscosity of the fracturing fluid (2.5 mPa·s) matches the low-viscosity fracturing fluid system used in the block.

(4) Proppant parameters

For a single-stage proppant used in coalbed methane well fracturing, the dosage typically ranges from 20 to 100 g/L. In this experiment, two proppant dosages, 60 and 20 g/L, are set. The proppant particle size used in the experiment is selected to match the commonly used particle size in the field.

Based on the above parameters, the experimental design is summarized in Table 3. The proppants used for temporary plugging are shown in Figure 5. To simulate the underground tri-axial stress environment and vertical well completion method, a small-scale true tri-axial fracturing simulation system is employed. Vertical stress (σ_v), maximum horizontal stress (σ_H), and minimum horizontal stress (σ_h) are applied along the X, Y, and Z directions, respectively. The wellbore direction aligns with the vertical stress (*X*-axis). The prepared core samples are placed in the core chamber, connected with pipelines, and subjected to the aforementioned tri-axial stress.

3.4 Quantitative characterization of fracture complexity

To facilitate a quantitative comparison of the impact of different experimental conditions on hydraulic fracture complexity, Eq. 3.3 is employed to calculate the complexity coefficient of the fractures.

$$F_c = n \times \frac{l_r}{l} \times \frac{\hbar_r}{\hbar} \tag{3.3}$$

F_c represents the fracture complexity coefficient (dimensionless). n is the number of fractures. l_r and l represents the actual length of the crack and the length of the straight line extended by it. h_r and h represents the actual height of the crack and the linear distance of its extension, cm.

4 Results and discussion

4.1 Comparison of post-fracture morphology in coal and rock samples at different depths

With the increase in depth, the *in situ* stress state, coal body structure, and coal-rock properties continuously change, resulting in significant differences between deep and shallow coal seams (Zhang

TABLE 3 Parameters used in fracturing experiments.

Sample number	Core sampling depth	Earth stress/ (MPa)			Fracturing fluid viscosity/ (mPa·s)	Injection rate/ (mL/min)	Number of temporary stops	Parameters of temporary plugging agent	
		σ_v	σ_H	σ_h				Concentration of TPA/(g/L)	Size of TPA/ (Mesh)
1	850	12	8	5	2.5	20	1	60	200/400
2	2,200~2,300	16	16	10	2.5	20	1	60	200/400
3		16	16	10	2.5	20	1	20	200/400
4		16	16	10	2.5	20	2	60	①200/400
									②10//20

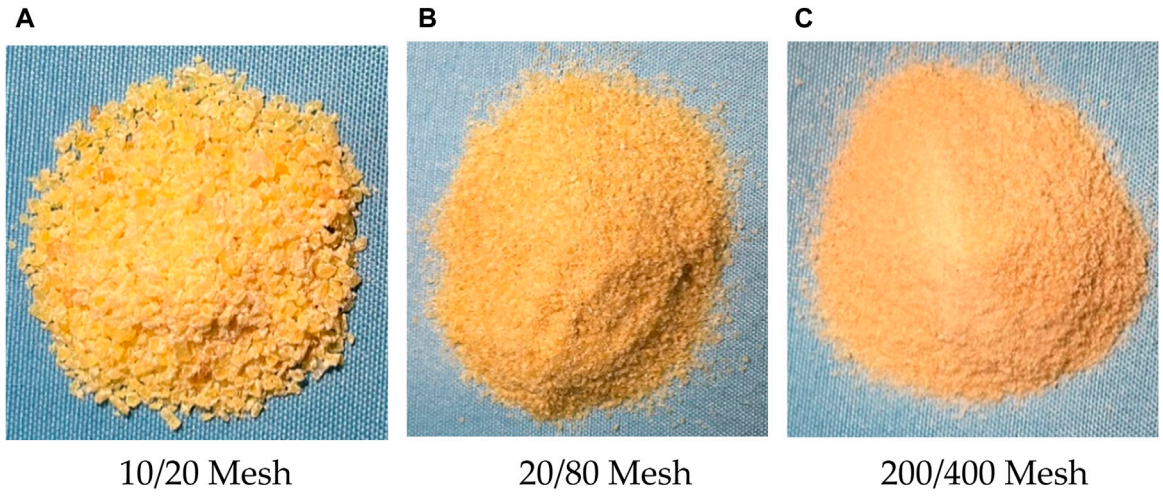

FIGURE 5
Temporary plugging agents with different particle sizes. **(A)** 10/20 Mesh **(B)** 20/80 Mesh **(C)** 200/400 Mesh.

et al., 2020; Xu et al., 2021; Zhou et al., 2022; Yong et al., 2023). This set of experiments aims to investigate the distinctions in post-fracturing fracture morphology between deep and shallow coal seams. The pre-fracturing CT scan images of Sample 1 and Sample 2 are illustrated in Figures 6, 7, respectively. It is evident that the internal fracture system of Sample 1 before fracturing is more complex, while Sample 2 exhibits more developed cleavage and cleats.

In the surface crack morphology diagrams, the initial hydraulic fracturing and secondary temporary plugging hydraulic fracturing traces are delineated by red and blue dashed lines, respectively. To facilitate a more efficient comparative analysis of the hydraulic fracture morphology of each specimen, three-dimensional reconstruction of the hydraulic fracture in the specimens was conducted using SOLIDWORKS software, visually presenting the hydraulic fractures within the specimens in three-dimensional space (Zheng et al., 2015). The hydraulic fracture morphology resulting from the TPDF of Specimens 1 and 2 is depicted in Figures 8, 9. In Sample 1, a primary crack initiated along the direction of minimum principal stress and vertically traversed the S1 and S6 planes. Temporary plugging diverted hydraulic fracturing resulted in the formation of a transverse crack and a branching crack occurred due to redirection at the naked eye section. The total area of artificial cracks was 249 cm^2, with a complexity coefficient of 4.34. In Sample 2, primary cracks uniformly originated from the wellbore and extended vertically to the S1 plane. Temporary plugging diverted hydraulic fracturing produced two redirected cracks—one parallel and one perpendicular to the wellbore—and a crossing branching crack developed at the S5 plane. The total area of artificial cracks was 203 cm^2, with a complexity coefficient of 5.88, which is 1.54 higher than that of Sample 1.

Comprehensive comparison of the pre-fracturing CT scans and post-fracturing crack morphology images for Sample 2 and Sample 1 reveals that the cracks formed after fracturing in Sample 1 have a longer extension distance, communicating with various surfaces of the rock specimen, but the crack morphology is relatively simple. In contrast, the cracks formed after fracturing in Sample 2 are predominantly vertical cracks extending along the direction

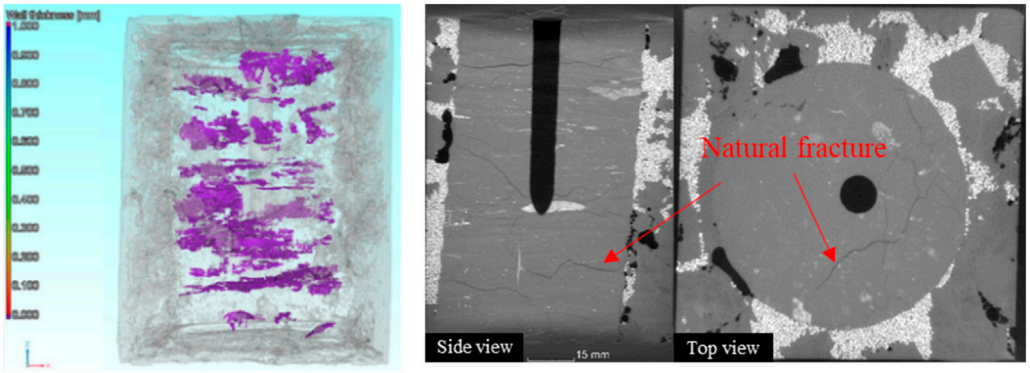

FIGURE 6
CT scan of sample 1 before pressure.

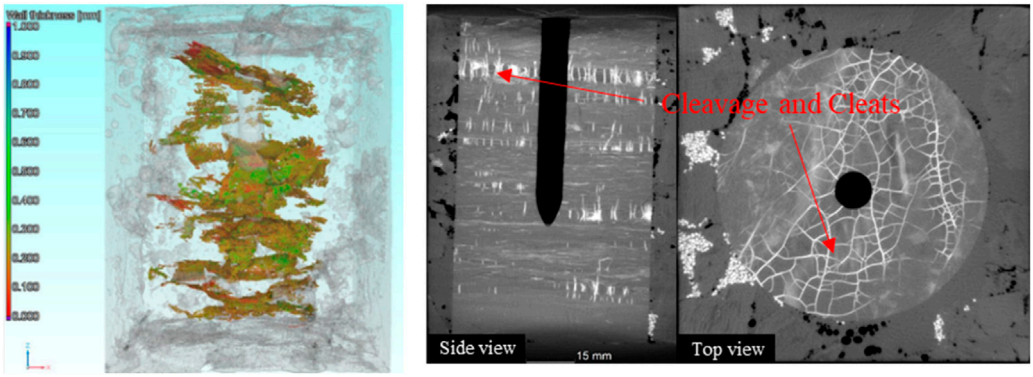

FIGURE 7
CT scan of sample 2 before pressure.

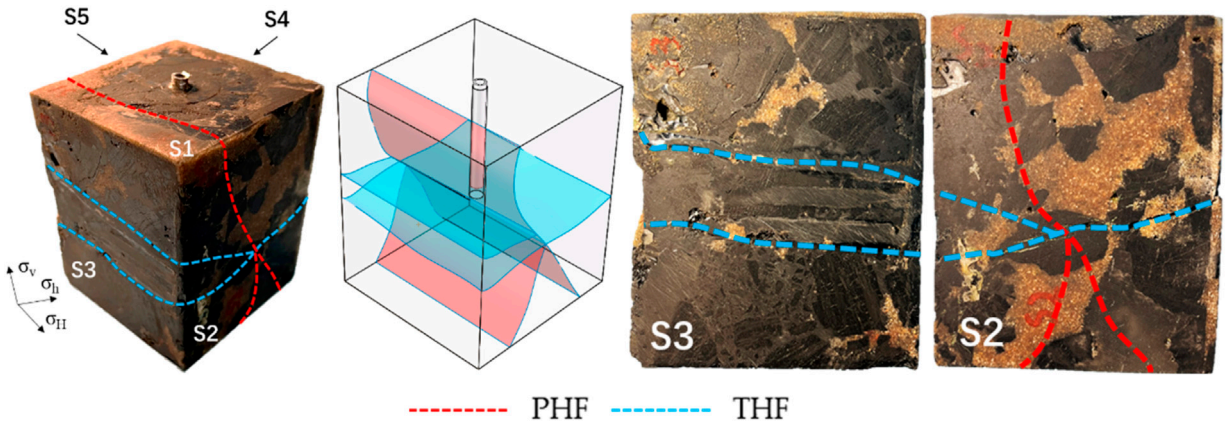

FIGURE 8
Surface crack morphology and internal crack reconfiguration of specimen 1.

of maximum principal stress, displaying a more complex morphology. However, these cracks are shorter and do not extend to the S3 and S6 surfaces. This is mainly due to the well-developed natural joints and cleavage inside Sample 2, which hinder the extension of artificial fractures in the designated direction and make them more prone to redirection. From this

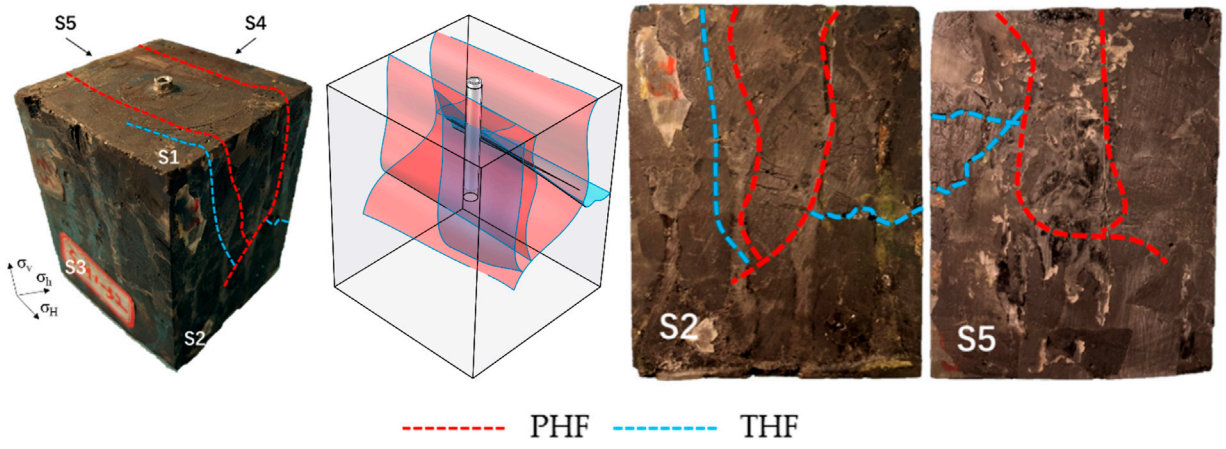

FIGURE 9
Surface crack morphology and internal crack reconfiguration of specimen 2.

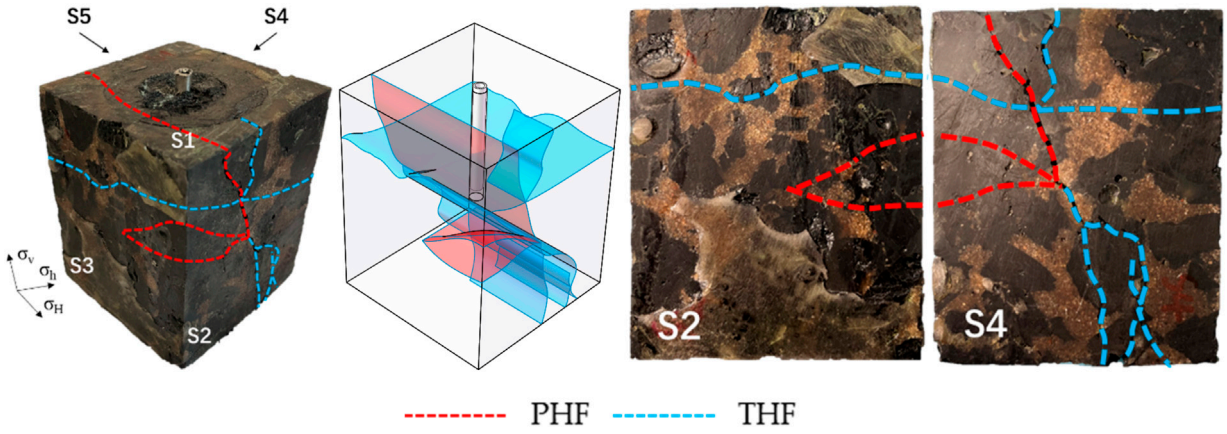

FIGURE 10
Surface crack morphology and internal crack reconfiguration of specimen 3.

analysis, it can be inferred that the natural joints and cleavage in the interior of deep coal rock specimens are more developed, hindering the extension of artificial fractures and making them more likely to undergo redirection. The fractures formed during hydraulic fracturing are mostly convoluted short cracks, and the overall transformation effects of both PF and TPDF on the rock specimen are not satisfactory.

4.2 Influence of TPA dosage on fracture morphology

During the TPDF, the quantity of TPA used can also influence the morphology of fractures to some extent (Liu et al., 2005; Xu et al., 2021; Shi et al., 2022; Wu et al., 2022; Zhou et al., 2022; Fang et al., 2023). In order to investigate the impact of the quantity of TPA on the expansion morphology of fractures in deep coal rock, this set of experiments increased the amount of TPA from 30 to 60 g/L for Specimen 3 and conducted a comparative analysis of the fracture morphology after temporary blocking fracturing.

As depicted in Figure 10, Sample 3 exhibited a complex network of multiple branching cracks following temporary plugging diverted hydraulic fracturing. Secondary cracks frequently redirected and extended to various surfaces of the specimen. The total area of artificial cracks measured 343 cm^2, with a complexity coefficient of 6.98, representing a 1.1 increase compared to Sample 2. This set of TPDF experiments significantly enhances the extension distance of fractures and, to a certain extent, overcomes the constraints imposed by natural joints and cleavage in the interior of deep coal rock. A comparison between Sample 2 and Sample 3 experiments reveals that increasing the concentration of the TPA is beneficial for increasing the number of redirections of artificial fractures, inducing the continued expansion of secondary fractures toward weaker planes, communicating with unmodified areas, and improving the modification effects of TPDF in previously untouched zones. This also results in an increased reservoir modification volume.

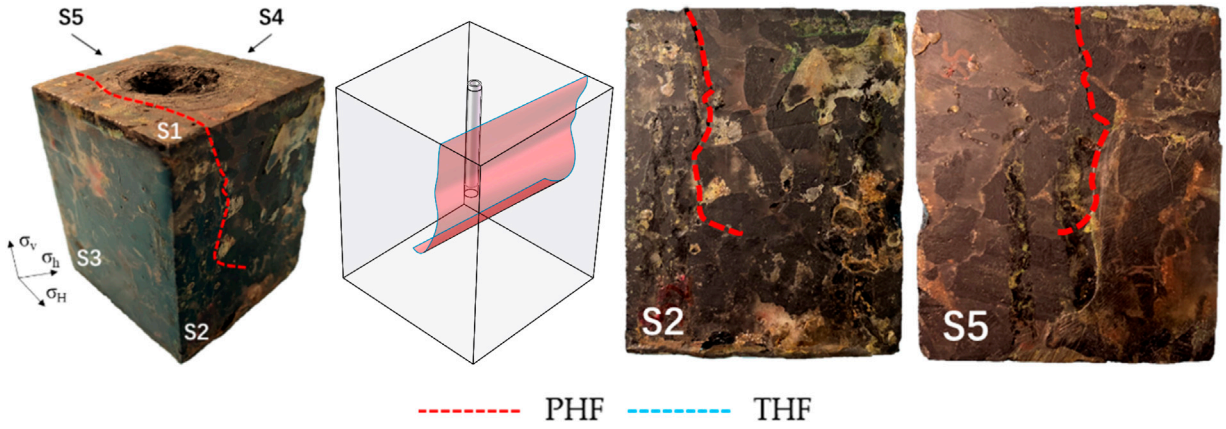

FIGURE 11
Surface crack morphology and internal crack reconfiguration of specimen 4.

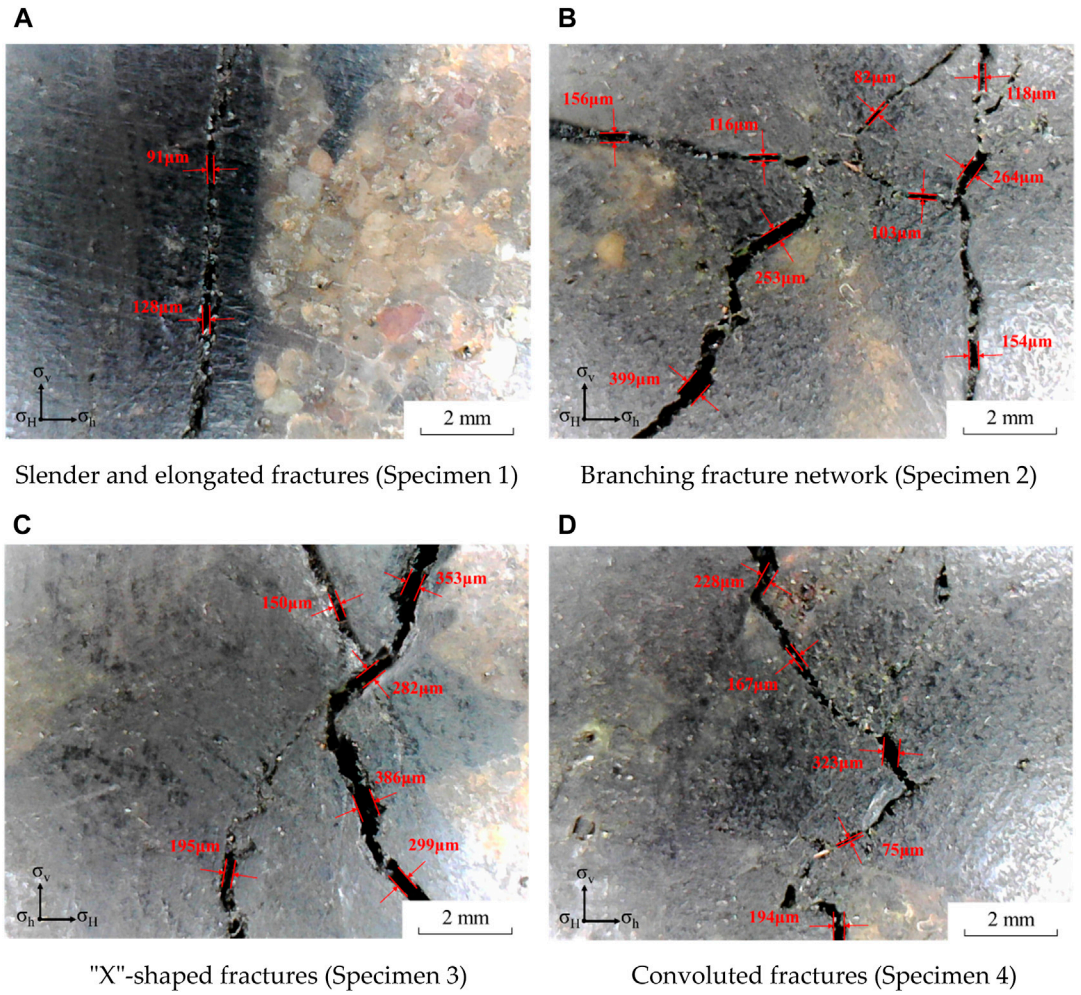

FIGURE 12
Typical local crack morphology and crack width variation of each specimen surface. **(A)** Slender and elongated fractures (Specimen 1) **(B)** Branching fracture network (Specimen 2) **(C)** "X"-shaped fractures (Specimen 3) **(D)** Convoluted fractures (Specimen 4).

4.3 Impact of TPA particle size on fracture morphology

The particle size of the TPA is also a crucial factor influencing the reservoir transformation effect of TPDF (Xiang, 2014; Jianguo et al., 2020; Lu, 2020; Liu et al., 2021; Ming et al., 2021; Shi et al., 2022; Zhang et al., 2022; Guo and Guo-Chuan-Ji, 2023; Wang et al., 2024). In order to study the impact of TPA particle size on the expansion morphology of fractures in deep coal rock, this set of experiments involved two rounds of TPDF, using 200/400 mesh (small particle size) and 10/20 mesh particle size (large particle size) temporary blocking agents for Specimen 4.

As shown in Figure 11, the initial fracture in Specimen 4 originated from the wellbore and extended vertically to the S1 surface. During the first round of TPDF using the 200/400 mesh small particle size TPA, there was no significant rupture pressure, and the temporary blocking agent did not effectively seal the initial fracture, failing to generate new artificial fractures. The total area of artificial cracks measured 58 cm^2, with a complexity coefficient of 1.26. In the second round of TPDF using the 10/20 mesh large particle size TPA, the rupture pressure was exceptionally high. The large particle size of the TPA led to excessive sealing near the wellbore, causing extensive fracturing of the coal rock near the wellbore and accumulating a large amount of coal dust. Overall, the TPDF transformation effect of Specimen 4 was poor, and the produced coal dust degraded the physical properties of the coal rock. The blockage of some flow channels reduced permeability, causing certain damage to the reservoir.

Comparing the two sets of experiments, Specimens 4 and 2, it can be observed that the choice of TPA particle size during deep coal rock TPDF is crucial. A TPA particle size that aligns better with the reservoir fracture system results in more effective TPDF. A particle size that is too small may fail to seal the fractures, making it difficult for the fractures to reorient. Conversely, when the particle size is too large, excessive wellbore sealing can lead to rapid pressure buildup, and the generated coal dust can damage the coal rock formation.

4.4 Analysis of typical local fracture morphology and fracture width in artificial fractures

The typical local fracture morphologies for each specimen are depicted in Figure 12. In Specimen 1, artificial fractures exhibit slender and elongated features, with fractures extending outward from the center of the S2 surface showing a narrowing trend in width. The average width of secondary fractures is 93 μm. Specimens 2 and 3, after temporary blocking fracturing, display complex intersecting fractures. In the central region of the intersecting area, the width of fractures extending outward tends to widen. The average widths of secondary fractures in Specimens 2 and 3 are 191 μm and 275 μm, respectively. It can be observed that, compared to shallow coal rock specimens, artificial fractures in deep coal rock specimens are more complex, with wider widths. Additionally, the width of fractures in the process of extension exhibits more frequent and significant variations. Increasing the quantity of TPA can widen the artificial fractures in deep coal rock during temporary blocking reorientation fracturing, enhancing the transformation effect. The initial fractures in Specimen 4 exhibit a convoluted expansion morphology, but due to the mismatch in the particle size of the TPA with the initial fractures, there is no apparent development of secondary fractures after the temporary blocking fracturing experiment.

5 Conclusion

This study employed a true triaxial hydraulic fracturing device, combined with CT scanning and crack reconstruction technology, to conduct PF and TPDF experiments on deep and shallow coal rock samples. The aim was to investigate the differences in internal structures between deep and shallow coal seams and the varying patterns of temporary blocking reorientation fracture expansion. Additionally, the study explored the influence of TPA quantity and particle size on the expansion of TPDF fractures in deep coal seams. The following conclusions were drawn.

(1) Deep coal rock samples exhibit more developed cleavage and cleats, which, to a certain extent, constrain the extension of artificial fractures. This hinders the opening and communication of natural weak planes. Post-fracturing cracks are predominantly vertical fractures initiated along the direction of maximum horizontal principal stress. These fractures tend to be wider but shorter in length, resulting in relatively complex fracture patterns and suboptimal transformation effects in the far-wellbore region.
(2) Increasing the dosage of the TPA can increase the number of redirections of fractures, facilitating communication with previously untouched areas, widening secondary fractures, and enhancing the overall modification effects of TPDF on the specimen. This leads to an increased reservoir modification volume.
(3) Suitable TPA particle size can effectively form plugging, which is conducive to inducing the steering and expansion of cracks. When the diameter of TPA is too small (200/400 mesh), it is difficult to form effective plugging, and the effect of temporary plugging fracturing is poor. When the particle size of the TPA is too large (10/20 mesh), it is easy to block the wellbore, causing destructive fracturing near the wellhead, producing a large amount of coal powder, and causing damage to the physical properties of the reservoir.

Data availability statement

The original contributions presented in the study are included in the article/supplementary material, further inquiries can be directed to the corresponding author.

Author contributions

ZS: Writing–original draft, Writing–review and editing. ZT: Writing–original draft, Writing–review and editing. LJ:

Writing–original draft, Writing–review and editing. AQ: Writing–original draft, Writing–review and editing. ZY: Writing–original draft, Writing–review and editing. SL: Writing–original draft, Writing–review and editing. ZZ: Writing–original draft, Writing–review and editing.

Funding

The author(s) declare that financial support was received for the research, authorship, and/or publication of this article. The authors are grateful for the financial support from the Key Technologies for Exploration and Development of Unconventional Natural Gas on Land in CNOOC's '14th Five Year Plan' Major Science and Technology Project (Grant No. KJGG2022-1002).

Conflict of interest

Authors ZS, ZT, JL, and QA were employed by China United Coalbed Methane Corporation Ltd.

The remaining authors declare that the research was conducted in the absence of any commercial or financial relationships that could be construed as a potential conflict of interest.

Publisher's note

References

Abass, H. H. (1990). Experimental observations of hydraulic fracture propagation through coal blocks. *SPE Conf. Pap.*, 21289.

Beugelsdijk, L. J., Pater, C. J., and Sato, K. (2000). "Proceedings of the SPE asia pacific conference on integrated modelling for asset management," in Society of Petroleum Engineers Conference Paper, SPE–59419–MS, London, UK, February 2000.

Cheng, Y., and Guo, P. (2013). Permeability prediction in deep coal seam: a case study on the No. 3 coal seam of the southern qinshui basin in China. *Sci. World J.* 2013, 1–10. doi:10.1155/2013/161457

Fang, Y., Fang-Xiong, Zhang-Lijuan, Pan-Xingen, Feng-Pandeng, Luo-Lei, W., et al. (2023). Development and performance test of an expansive particle temporary plugging agent. *J. Phys. Conf. Ser.* 2539, 012014. doi:10.1088/1742-6596/2539/1/012014

Fu, N., Yang, S., He, Q., et al. (2016). Efficient accumulation conditions of tight sand gas in linxing-shenfu block on the eastern margin of Ordos Basin. *Acta Pet. Sin.* 37 (S1), 111–120.

Gao, L., Xie, Y., Pan, X., et al. (2018). Analysis of gas content and geological model of deep coalbed methane in linxing. *J. China Coal Soc.* 43 (06), 1634–1640.

Guo, C.-J., and Guo-Chuan-Ji, R. (2023). Experimental study on microstructure of temporary plugging zone and relevant plugging capacity based on CT images within different particulates sizes. *SPE Conf. Pap.*

Guo, M. (2016). Characteristics of hydrocarbon source rocks in the linxing-shenfu area on the northeastern margin of the Ordos Basin. *China Coalbed Methane* 13 (03), 13–17.

Guo, M. (2020). Influence of reservoir space types on macro properties: a case study of linxing-shenfu area in east Ordos. *China Coalbed Methane* 17 (02), 18–23.

Haifei, X., Zhu, G., Zhang, J., et al. (2019). Research and application of hydraulic wave and fracturing technology in deep coalbed methane. *Coal Technol.* 38 (05), 81–84.

Hou, E., Xie, X., Wang, S., et al. (2021). Research on the development law of surface fractures in medium-buried coal seam mining. *J. Min. Saf. Eng.* 38 (06), 1178–1188.

Huang, S., Liu, W., and Zhao, G. (2009). Current status and development trends of coalbed methane development and utilization in China. *China coal.* 35 (01), 5–10.

Huang, Z., Guofu, L., Yang, R., et al. (2022). Current status and development trends of coalbed methane development technology in China. *J. China Coal Soc.* 47 (09), 3212–3238.

Jia, D., Zhu, G., Yong, L., et al. (2022). Challenges and technical countermeasures for exploration and development of tight sandstone gas reservoirs on the margin of Ordos Basin: a case study of linxing-shenfu gas field. *Nat. Gas. Ind.* 42 (01), 114–124.

Jianguo, S., Yang, Y., Wang, L., et al. (2020). Research on injection device of ultra-large particle temporary plugging agent. *Oil Field Equip.* 49 (06), 74–78.

Kuuskraa, V. A., and Wyman, R.-E. (1993). Deep coal seams: an overlooked source for long-term natural gas supplies. *SPE Conf. Pap.*

Huanhuan, L. (2020). Optimization of deep coalbed fracturing process in linxing-shenfu block. Master's thesis, China University of Petroleum (Beijing, China).

Lijun, M., and Zhu, G. (2021). Geological characteristics and exploration breakthrough of tight gas fields in linxing-shenfu area on the northeastern margin of Ordos Basin. *China Offshore Oil Gas* 34 (04), 16–29.

Liu, D., Zhou, J., Qisen, G., et al. (2021). Research on temporary blocking and reorientation hydraulic fracturing technology in underground coal mines. *Mod. Coal Mines* (01), 102–105.

Liu, G., Pang, F., and Chen, Z. (2000). Similarity criteria in hydraulic fracturing simulation experiments. *J. Univ. Petroleum Ed. Nat. Sci.* 45-48 (05), 6–5.

Liu, Q., Yao, H., Liu, P., et al. (2005). Research on calculation method of temporary blocking agent dosage in fracturing construction. *Daqing Petroleum Geol. Dev.* (06), 58–59.

Lu, X. (2017). "Study on the geological peculiarity and productivity influencing factors of deep coalbed methane in the southern part of qinshui basin,". Master's thesis (Beijing, China: China University of Geosciences).

Lu, Z. (2020). Research progress and prospect of temporary plugging agent for reorientation fracturing. *Sci. Technol. Eng.* 20 (31), 12691–12701.

Ming, L., Guo, J., Gou, K., Mu, T., and Zhang, H. (2021). Numerical study on mechanism and parameters optimization of temporary plugging by particles in wellbore. *SPE Prod. Operations* 37, 135–150. doi:10.2118/208585-pa

Qin, Y., Shen, J., and Xiaogang, L. (2022). Analysis of the degree and reliability of coalbed methane resources in China. *Nat. Gas. Ind.* 42 (06), 19–32.

Shi, S., Zhang, T., Wang, M., Wang, J., Wang, J., Wang, Z., et al. (2022). Study on field test and plugging simulation of the knot temporary plugging agent. *Chem. Technol. Fuels Oils* 58, 530–543. doi:10.1007/s10553-022-01417-0

Sun, Q., Zhao, Q., Jiang, X., et al. (2021). Prospects and countermeasures of coalbed methane exploration and development in China under the new situation. *J. China Coal Soc.* 46 (01), 65–76.

Tao, W., Zhang, Z., Niu, Z., et al. (2018). Analysis of reservoir properties and development engineering differences in deep and shallow coalbed methane reservoirs. *Coal Technol.* 37 (02), 58–60.

Wang, D., Zheng, B., Liu, K., Yang, Z., and Zhou, (2024). Comparative experimental investigation on permeability and pressure bearing capacity of different types of temporary plugging bodies. *Unconv. Resour.* 4, 100062. doi:10.1016/j.uncres.2023.08.004

Wu, J. (2022). Analysis of main geological factors in deep coalbed methane mining. *Inn. Mong. Coal Econ.* (23), 65–67.

Wu, X., Song, Z., Zheng, B., Zhang, K., and Zhou, H. (2022). A review on mechanism and adaptive materials of temporary plugging agent for chemical diverting fracturing. *J. Petroleum Sci. Eng.* 212, 110256. doi:10.1016/j.petrol.2022.110256

Wuzhong, L., Wang, Y., Sun, B., et al. (2004). Distribution and prospects of coalbed methane resources in China. *Nat. Gas. Ind.* 8-10 (05), 143–144.

Xiang, Li (2014). Experimental study on the application of temporary plugging agent in fracturing construction. *Liaoning Chem. Ind.* 43 (08), 987–988.

Xianqing, L., Baolin, H., Zhang, X., Zhang, J., He, Y., et al. (2019). Reservoir characteristics and coalbed methane resource evaluation of deep-buried coals: a case study of the No.13–1 coal seam from the panji deep area in huainan coalfield, southern north China. *J. Petroleum Sci. Eng.* 179, 867–884. doi:10.1016/j.petrol.2019.04.100

Xie, B., Zou, P., Luo, W., et al. (2018). Study on coalbed methane accumulation conditions. *Inn. Mong. Coal Econ.* (07), 150–151.

Xu, J., Liu, G., and Wang, Y. (2021). Technology of temporary blocking and reorientation fracturing inside fractures in tight reservoirs. *Pet. Drill. Tech.* 43 (03), 374–378.

Yang, G. (2021). "Study on the genesis mechanism of high-quality reservoirs in upper paleozoic tight sandstones in the linxing-shenfu area,". Master's thesis (Beijing, UK: China University of Geosciences).

Yang, Z., He, R., Xiaogang, L., et al. (2017). Study and application of synchronous fracturing stress interference mechanism in deep coalbed methane. *Reserv. Eval. Dev.* 7 (04), 65–72.

Yong, L., Lifu, X., Zhang, S., et al. (2023). Differences in gas-bearing systems and development strategies for deep coal seams. *J. China Coal Soc.* 48 (02), 900–917.

Zhang, H., Shen, J., Kexin, L., et al. (2020). Characteristics of *in-situ* stress field and analysis of stress changes in the western area of linxing deep coalbed methane in Ordos Basin. *Geol. Prospect.* 56 (04), 809–818.

Zhang, K., Tang, X., Du, L., Yuan-Fujian, Z., and Zhou, F. (2022). Experimental study of the temporary plugging pattern of perforations by multi-particle size composites. *IOP Conf. Ser. Earth Environ. Sci.* 984, 012016. doi:10.1088/1755-1315/984/1/012016

Zhang, P., Wu, R., Hu, X., and Zhou, W. (2019). Dynamic monitoring the deformation and failure of extra-thick coal seam floor in deep mining. *J. Appl. Geophys.* 163, 132–138. doi:10.1016/j.jappgeo.2019.02.007

Zheng, X., Chen, M., Hou, B., et al. (2015). Three dimensional reconstruction of hydraulic fractures based on Solidworks Science. *Technol. Eng.* 15 (14), 32–38.

Zhou, F., Yuan, L., Liu, X., et al. (2022). Key technologies and progress in temporary blocking and reorientation fracturing. *Petroleum Sci. Bull.* 7 (3), 365–381.

Zou, Y., Shi, S., Zhang, S., et al. (2021). Experimental study on fracture conduction capacity of extra-thick gravel with sand fracturing — a case study of maru extra-thick gravel in junggar basin. *Petroleum Explor. Dev.* 48 (06), 1202–1209.